# Tuning of Copper(I)–Dioxygen Reactivity by Bis(guanidine) Ligands

**Sonja Herres-Pawlis,[a] Ulrich Flörke,[a] and Gerald Henkel*[a]**

*Dedicated to Professor H. W. Roesky on the occasion of his 70th birthday*

**Keywords:** Bioinorganic chemistry / Copper / Guanidine ligands / Ligand design / O–O activation

A series of bis(guanidine) ligands designed for use in biomimetic coordination chemistry, namely bis(tetramethylguanidino)-, bis(dipiperidinoguanidino)-, and bis(dimethylpropyleno)propane (btmgp, $DPipG_2p$ and $DMPG_2p$, respectively), has been extended to include bis(dimethylethyleneguanidino)propane ($DMEG_2p$), which has both $N^{amine}$ atoms of each guanidine functionality connected by a short ethylene bridge, as a member. From this series, a family of novel bis(guanidine)copper(I) compounds – $[Cu_2(btmgp)_2][PF_6]_2$ (**1**), $[Cu_2(DPipG_2p)_2][PF_6]_2$ (**2**), $[Cu_2(DMPG_2p)_2][PF_6]_2$ (**3**), and $[Cu_2(DMEG_2p)_2][PF_6]_2 \cdot 2MeCN$ (**4**) – has been synthesised. Single-crystal X-ray analysis of **1**–**4** demonstrated that these compounds contain dinuclear complex cations that contain twelve-membered heterocyclic $Cu_2N_4C_6$ rings with the Cu atoms being more than 4 Å apart. Each copper atom is surrounded by a set of two N-donor functions from different ligands, resulting in linear N–Cu–N coordination sites. Depending on their individual substitution patterns, the guanidine moieties deviate from planarity by characteristic propeller-like twists of the amino groups around their $N–C^{imine}$ bonds. The influence of these groups on the reactivity of the corresponding complexes **1**–**4** with dioxygen was investigated at low temperatures by means of UV/Vis spectroscopy. The reaction products can be classified into $\mu$-$\eta^2$:$\eta^2$-peroxodicopper(II) or bis($\mu$-oxo)dicopper(III) complex cations that contain the $\{Cu_2O_2\}^{2+}$ core portion as different isomers. The electronic properties of the specific bis(guanidine) ligands are discussed from the viewpoint of their $\sigma$-donor and $\pi$-acceptor capabilities, and it is shown that $\mu$-$\eta^2$:$\eta^2$-peroxodicopper(II) complexes are stabilised relative to the bis($\mu$-oxo)dicopper(III) ones if $\pi$ conjugation within the guanidine moieties is optimised.


## Introduction

Dioxygen binding in biology is controlled by appropriately designed transition metal active sites. Investigations directed towards an understanding of the mechanisms and a transformation of such processes to technical applications are among the most important research objectives not only in bioinorganic chemistry but also in numerous and diverse arrays of catalytic oxidation reactions.[1–7]

From X-ray structure determinations of the blood dioxygen carrier hemocyanin (for example in arthropods and molluscs)[7,8] it is known that the protein active sites consist of $\mu$-$\eta^2$:$\eta^2$-peroxodicopper(II) units where each copper ion binds three supporting exogenic N-donor functions originating from histidine imidazole groups. Spectroscopic comparisons suggest that this binding mode occurs also in tyrosinases (phenol → *o*-quinone)[9] and catechol oxidases (*o*-catechol → *o*-quinone).[10,11] $Cu–O_2$ (1:1) adducts are suggested to be involved in the activities of dopamine β-hydroxylase,[12] peptidylglycine α-hydroxylating monooxygenase[1b] and amine oxidases,[12,13] and units containing three copper atoms are found in multicopper oxidases (MCOs) that reduce $O_2$ to water.[9a]

An understanding of the nature of these reactive intermediates is essential in order to use their principles in coordination chemistry directed towards catalytic applications. Considerable progress towards this aim has been attained through examination of the dioxygen reactivity of synthetic $Cu^I$ complexes, which has resulted in the characterisation of a variety of systems containing $\mu$-$\eta^2$:$\eta^2$-peroxodicopper(II), bis($\mu$-oxo)dicopper(III) and bis($\mu_3$-oxo)tricopper(III,II,II) complex topologies (Figure 1).

A key research objective has been to understand how supporting ligand structural features influence the relative stabilities and interconversions of these species, and especially the effects that control the equilibrium between the P- and O-core that are relevant to proposed metalloprotein active-site intermediates. It has been shown that both units can be supported by neutral, multidentate N-donor ligands and that ligand structural elements (e.g., size of substituents, donor type, bite angle, denticity) play a critical role in determining which units form and how they react.[1,2]

[a] Fakultät für Naturwissenschaften, Department Chemie, Universität Paderborn,
Warburger Strasse 100, 33098 Paderborn, Germany
Fax: +49-5251-603-423
E-mail: biohenkel@uni-paderborn.de
Supporting information for this article is available on the WWW under http://www.eurjic.org or from the author.

 **DOI: 10.1002/ejic.200400822**  

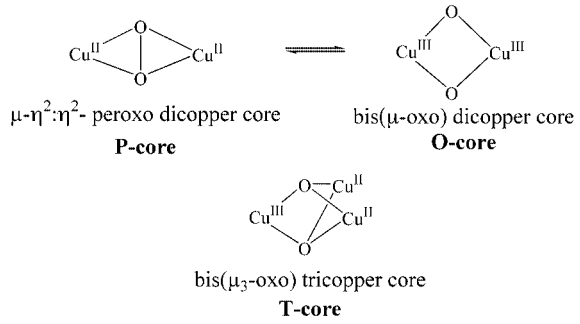


Figure 1. Topologies of $Cu/O_2$ species where each Cu atom is bonded to both O atoms simultaneously.

The majority of model complexes that imitate the native system make use of tridentate N-donor ligands for copper complexation. These ligands are able to stabilise the $Cu_2O_2$ core portion by forming square-pyramidal $CuO_2N_3$ coordination sites with more weakly bonded axial N-donor functions.[3,14,15] However, model complexes that mimic tyrosinase activity are not necessarily dependent on these facial-capping ligands. As has been shown by Stack et al., bidentate N-donor ligands are also capable of forming complexes containing the heterocyclic $Cu_2O_2$ core portion.[4,16,17] The associated square-planar $CuO_2N_2$ coordination sites are expected to be more accessible for external substrates that may act as targets for catalytic oxygenation reactions.[18–20] Following this approach, peralkylated diamine ligands have been used to stabilise either the bis(μ-oxo)dicopper(III) (O-core complexes) or the μ-$\eta^2$:$\eta^2$-peroxodicopper(II) core portion (P-core complexes) depending on the type of substituents.[2a] These systems exhibit tyrosinase-like reactivity as they insert oxygen into C–H bonds. Although the O-core has yet not been detected in enzymatic systems, its relevance for hydroxylation activity seems likely because the equilibria between P- and O-core states proven for model complexes have to be taken into account.[3,16,21–23]

In our search for bifunctional N-donor ligands able to stabilise unusually high metal oxidation states we extended our interest towards guanidine-type systems. Following this approach, bis(tetramethylguanidino)propane (btmgp) was synthesised as the first member of a series of bifunctional peralkylated guanidine ligands designed for use in biomimetic coordination chemistry.[24–26] Attempts to modify the guanidine moieties resulted in the successful preparation of the novel derivatives bis(dimethylpropyleneguanidino)propane ($DMPG_2p$), bis(dipiperidylguanidino)propane ($DPipG_2p$) and bis(dimethylethyleneguanidino)propane ($DMEG_2p$) (Figure 2).[27a,27c]

In this paper we describe a series of dinuclear copper(I) complexes containing these ligands and their reaction behaviour towards molecular oxygen. Depending on the residues attached to the guanidine systems, the resulting $Cu_2O_2$ species are either bis(μ-oxo)dicopper(III) or μ-$\eta^2$:$\eta^2$-peroxodicopper(II) complexes.

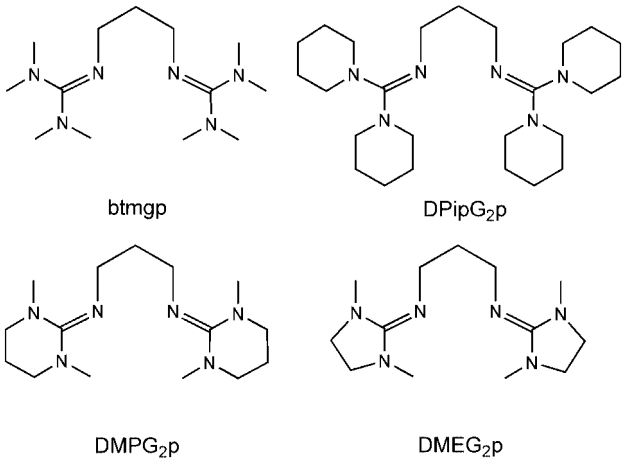


Figure 2. Guanidine-based bifunctional N-donor ligands.

## Results and Discussion

### Synthesis of the Ligands

The synthesis of the ligands was accomplished according to a general procedure that allows the condensation of almost every urea with an amine to form a guanidine compound via the corresponding Vilsmeier salt.[27b] The Vilsmeier salt is obtained in good yield by reaction of the substituted urea with phosgene in toluene or acetonitrile (Scheme 1).

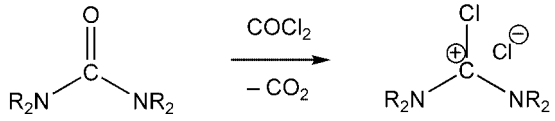


Scheme 1. Generation of the Vilsmeier salts.

The reaction of the Vilsmeier salt with propylene-1,3-diamine, in the presence of triethylamine as an auxiliary base, leads to the corresponding guanidine after deprotonation of the initially formed hydrochloride (Scheme 2). Separation from the by-product $Et_3NHCl$ is accomplished by adding 1 equiv. of NaOH per guanidine functionality and removing the resulting $NEt_3$ and solvent under reduced pressure. The hydrochloride is not isolated but deprotonated in a two-phase system of MeCN/50% aqueous KOH in order to obtain the pure free base, which needs no further purification.

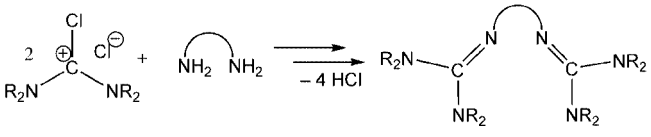


Scheme 2. Reaction between the Vilsmeier salt and the bis(amine).

### Synthesis of the Copper Complexes

The complexes were synthesised in good yields by combining $[Cu(MeCN)_4][PF_6]$ with 1.05 equiv. of the bis(guani-

  

dine) ligand in dry acetonitrile and stirring for 30 min (Scheme 3). The resulting complex salts **1**–**4** are soluble in polar aprotic media such as MeCN, $CH_2Cl_2$ and THF, but insoluble in diethyl ether and hydrocarbons.

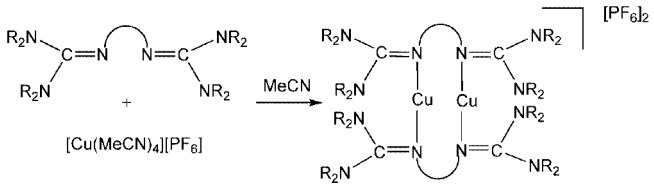


Scheme 3. Complexation of $[Cu(MeCN)_4][PF_6]$ with bis(guanidine) ligands.

All compounds are extremely sensitive to air and moisture due to the high proton affinity of guanidines, which is caused by delocalisation of the positive charge in the guanidine moiety.

## Crystal Structures

Single crystals of compounds **1**–**4** suitable for X-ray crystallography were grown by slow diffusion of diisopropyl ether into acetonitrile solutions. The results of the structural analyses are shown in Figures 3, 4, 5, and 6, respectively, while selected bond lengths and angles are collected in Table 1; parameters relating to the data collection and refinement can be found in the Experimental Section.

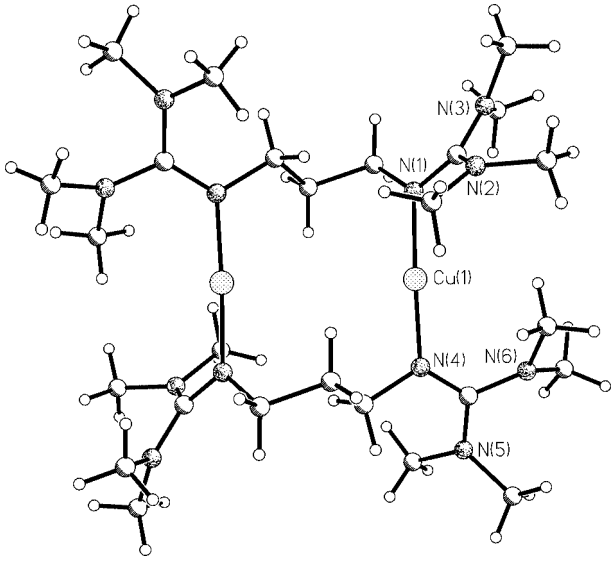


Figure 3. Structure of the $[Cu_2(btmgp)_2]^{2+}$ moiety in crystals of **1**.

The dinuclear complex cations present in all four compounds exhibit molecular ring structures with significant differences in the folding of their propylene chains and in their corresponding interligand H···H separations passing through the centroids of the molecules. The copper centres show almost linear twofold coordination from two N-donor atoms of different ligands with N–Cu–N angles of 176.66(9), 176.77(15), 177.15(6), and 175.29(9)° for **1**–**4**, respectively. The centroids of the molecules lie on crystallographic inversion centres, resulting in perfectly planar

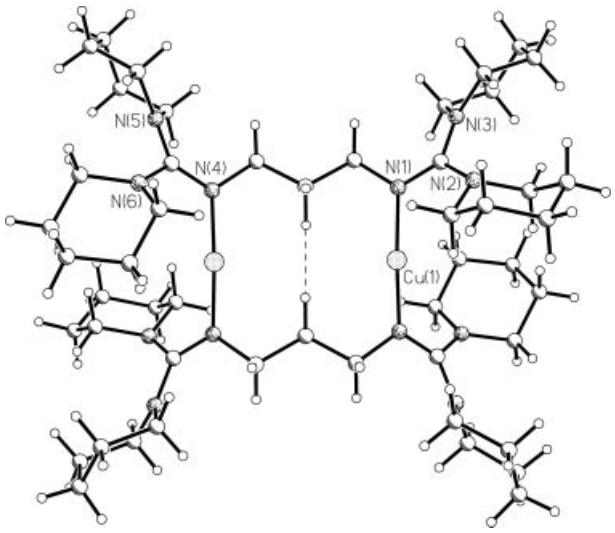


Figure 4. Structure of the $[Cu_2(DPipG_2p)_2]^{2+}$ moiety in crystals of **2**.

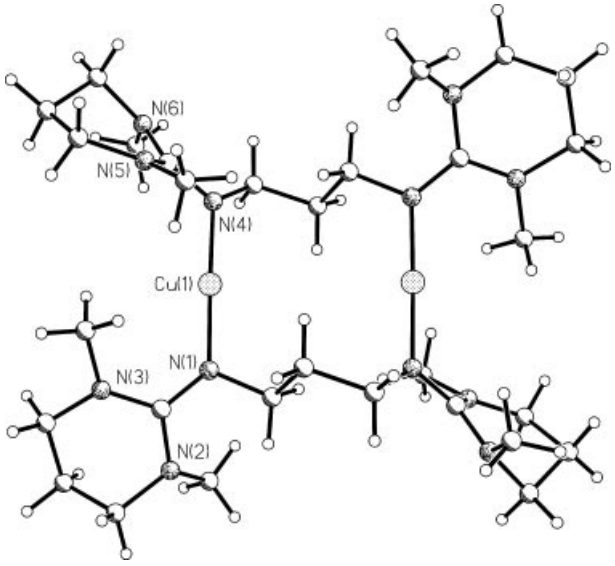


Figure 5. Structure of the $[Cu_2(DMPG_2p)_2]^{2+}$ moiety in crystals of **3**.

$Cu_2N_4$ moieties. The corresponding Cu–N, N=C, N–C and propyl-bridge C–C distances vary only very slightly from **1** to **4** and are almost identical (averaged values in the order from **1** to **4**): Cu–N: 1.877, 1.866, 1.869, 1.875 Å; N=C: 1.319, 1.309, 1.324, 1.314 Å; C–N(guanidine): 1.358, 1.364, 1.357, 1.359 Å; N–C(propyl): 1.474, 1.471, 1.474, 1.474 Å; C–C(propyl): 1.523, 1.513, 1.523, 1.517 Å. The Cu–N–C and N–C–C ring angles vary slightly in a non-systematic manner, the C–C–C angles are 111.6(2)°, 115.6(3)°, 112.4(1)° and 112.7(2)° for **1**–**4**. These differences may be traced back to variations in the Cu···Cu separations [4.121(1), 4.723(1), 4.358(1), and 4.488(1) Å, respectively]. In **1**, the $N=C(N)_2$ planes of the guanidine moieties are nearly perpendicular to each other with a dihedral angle of 86.3°. For **3**, **2**, and **4** these angles decrease to 80.0°, 71.5° and 68.4°, respectively.

  

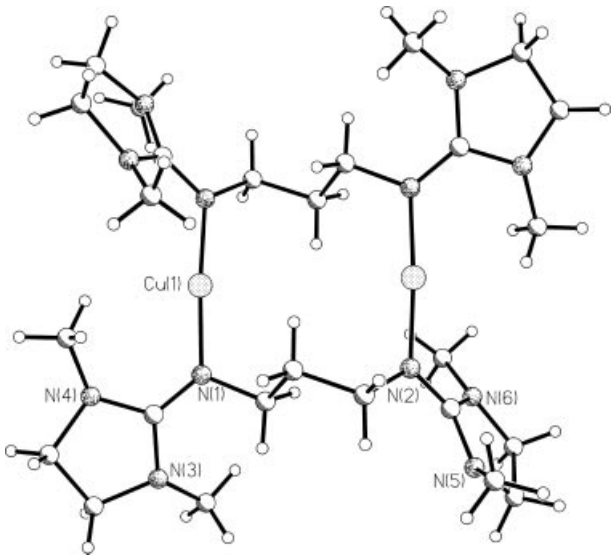


Figure 6. Structure of the $[Cu_2(DMEG_2p)_2]^{2+}$ moiety in crystals of **4**.

Table 1. Selected distances and angles of the complex cations in crystals of **1**–**4**.

| Distances [Å] | 1 | 2 | 3 | 4 |
|---|---|---|---|---|
| Cu···Cu | 4.121(1) | 4.723(1) | 4.358(1) | 4.488(1) |
| Cu–$N^{imine}$ | 1.876(2) | 1.876(3) | 1.872(1) | 1.878(2) |
| | 1.878(2) | 1.856(3) | 1.867(1) | 1.873(2) |
| N=C | 1.323(3) | 1.320(5) | 1.323(2) | 1.310(3) |
| | 1.315(3) | 1.297(4) | 1.325(2) | 1.318(3) |
| H···H[a] | 3.37 | 2.30 | 3.26 | 3.00 |
| Angles [°] | | | | |
| $N^{imine}$–Cu–$N^{imine}$ | 176.7(1) | 176.8(1) | 177.2(1) | 175.3(1) |
| $N^{amine}$–C–$N^{amine}$ | 116.0(2) | 114.7(4) | 117.5(1) | 110.0(2) |
| | 116.8(2) | 116.0(4) | 117.6(1) | 110.9(2) |

[a] Shortest H···H contact between parallel propylene spacer groups; the H–H vector passes through the centroid of the corresponding complex cation.

Compared with the free ligands $DMPG_2p$ and $DPipG_2p$,[27a] the C=N bonds in **2** and **3** are clearly elongated by about 0.04 Å, whereas the remaining geometric ring parameters show no relevant influence from copper complexation. The $N=C(N)_2$ planes in these ligands show dihedral angles of 23.1 and 31.5°.

Compared with the complexes **1**–**3** (116.4, 115.4, and 117.6°, respectively), the $N^{amine}$–C–$N^{amine}$ angle in **4** is diminished to 110.5° as the short ethylene linker in the $DMEG_2p$ ligand introduces steric strain.

Table 2 summarises the dihedral angles between the $CN_3$ guanidine plane and the $C^{imine}$–$N^{amine}$–$(C^{alkyl})_2$ planes within the guanidine moieties in the crystalline free bases and in the solid complex salts. It is assumed that the deviation of an individual angle from the mean value mainly reflects packing forces of the crystals. In solution, however, these angles are not subjected to anisotropic interactions with the solvent. For that reason, the following discussion is based on the assumption that the mean angle found in the crystalline state comes close to the situation in solution.

Table 2. Dihedral angles [°] between the $CN_3$ guanidine plane and the $C^{imine}$–$N^{amine}$–$(C^{alkyl})_2$ planes (mean values and ranges of individuals).

| Compound | Angle [°] |
|---|---|
| btmgp | n/a |
| $DPipG_2p$ | 40.7 [39.2–42.7] |
| $DMPG_2p$ | 25.9 [19.7–31.8] |
| $DMEG_2p$ | n/a |
| $[Cu_2(btmgp)_2][PF_6]_2$ (**1**) | 34.1 [32.3–35.9] |
| $[Cu_2(DPipG_2p)_2][PF_6]_2$ (**2**) | 37.6 [32.2–43.2] |
| $[Cu_2(DMPG_2p)_2][PF_6]_2$ (**3**) | 24.8 [16.7–33.5] |
| $[Cu_2(DMEG_2p)_2][PF_6]_2$ (**4**) | 17.4 [12.7–23.1] |

## UV/Vis Spectra

Upon reaction of **1** and **2** with $O_2$, intensive LMCT absorption bands at 300 ($\varepsilon$ = 15600) and 390 nm ($\varepsilon$ = 17200 $M^{-1}cm^{-1}$) are observed which are characteristic for all O-core complexes known so far (Figure 7).[28a] These species are unstable even at –80 °C in dichloromethane. The initial red solutions change to bluish-green upon warming up to room temperature within 1–2 h.

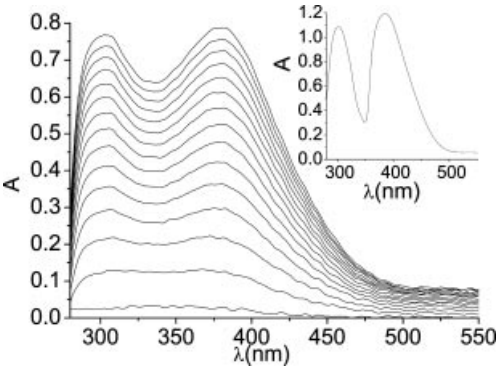


Figure 7. Time-dependent UV/Vis absorption spectra (every 2 min) observed upon introduction of $O_2$ gas into a $CH_2Cl_2$ solution of **2** (0.25 mM, –80 °C) during 30 min; inset: spectrum after 2 h (0.33 mM).

Compound **3** reacts with $O_2$ in dichloromethane with predominant formation of a P-core complex which can be identified by LMCT absorptions at 350 ($\varepsilon$ = 21200) and at 550 nm ($\varepsilon$ = 900 $M^{-1}cm^{-1}$). The band at about 300 nm ($\varepsilon$ = 13500 $M^{-1}cm^{-1}$) originates from O-core components that are formed concomitantly with the P-core (Figure 8). The O-core absorption at 390 nm is not resolved.

In contrast, reaction of **3** with $O_2$ in acetonitrile at –40 °C results in the immediate formation of an O-core complex, as shown by the UV/Vis absorption bands at 290 ($\varepsilon$ = 13000) and 390 nm ($\varepsilon$ = 15800 $M^{-1}cm^{-1}$; Figure 9). With MeCN as solvent, the equilibrium between P- and O-core is shifted almost completely to the O-core side. These results show that coordinating solvents are better suited to stabilise the O-core than non-coordinating ones, and thus confirm the reports of other groups.[1a,2,3a]

Treatment of a 0.2 mM solution of **4** in $CH_2Cl_2$ with dioxygen at –80 °C resulted in a green colour of the solution. At higher concentrations, the solution turns dark brown. The UV/Vis spectrum observed 1 h after introduction of

  

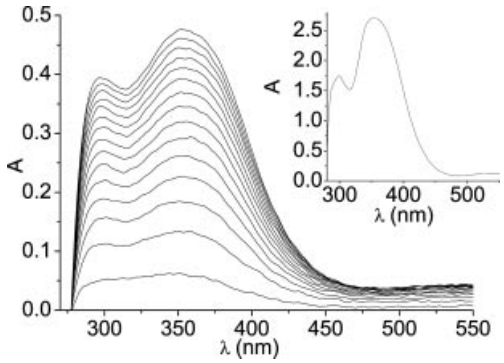


Figure 8. Time-dependent UV/Vis absorption spectra (every 2 min) observed upon introduction of $O_2$ gas into a $CH_2Cl_2$ solution of **3** (0.2 mM, –80 °C) during 30 min; inset: spectrum after 2 h (0.5 mM).

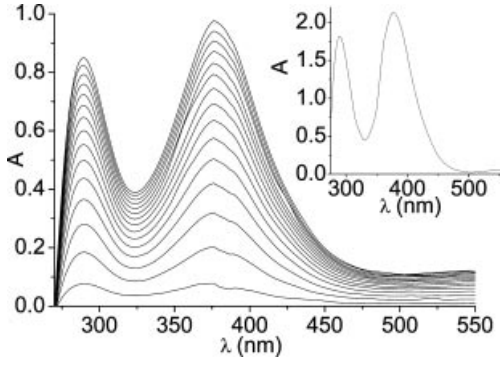


Figure 9. Time-dependent UV/Vis absorption spectra (every 30 s) observed upon introduction of $O_2$ gas into an MeCN solution of **3** (0.25 mM, –40 °C) during 8 min; inset: spectrum after 1 h (0.5 mM).

molecular oxygen is shown in Figure 10. The spectrum is dominated by a strong absorption band at 355 nm ($\varepsilon$ = 17000 $M^{-1}cm^{-1}$) indicative of the predominant formation of the P-core complex. The shoulder at 320 nm ($\varepsilon$ = 9500 $M^{-1}cm^{-1}$) is assigned to the formation of O-core contributors.

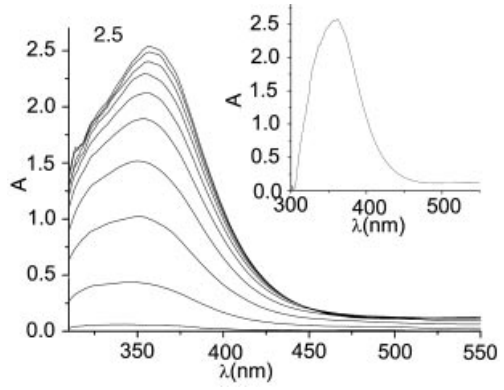


Figure 10. Time-dependent UV/Vis absorption spectrum (every 2 min) observed upon introduction of $O_2$ gas into a solution of **4** in MeCN/$CH_2Cl_2$ (1:10) (0.5 mM, –80 °C) during 30 min, inset: spectrum after 1 h (0.25 mM).

## Kinetic Aspects

The increase in the absorption bands during the reaction of **1**–**3** with dioxygen in excess obeys first-order kinetics (Figure 11). Moreover, the same first-order rate constants were obtained for reactions starting from different concentrations of **3** in $CH_2Cl_2$. This observation indicates that the reaction of the copper(I) complexes with oxygen is first-order with respect to the copper complex but of zero-order with respect to $O_2$ if it is used in excess. The activation parameters ($\Delta H^{\ddagger}$ and $\Delta S^{\ddagger}$) for the formation of the O-core complexes of **1** and **2** and the P-core complex of **3** were determined from the temperature dependence of $k$ (–40 to –80 °C). The first-order rate constants ($k$) determined at –80 °C and the activation parameters for the formation of the copper–dioxygen species are summarised in Table 3. The kinetic data given below are in accordance with comparable systems reported in the literature, which exhibit small activation enthalpies and very negative activation entropies.[22,23] A small activation enthalpy is indicative of the high driving force for the reaction of a copper(I) complex with dioxygen, whereas a negative activation entropy is the result of a reaction where two molecules are combined to form a new one.

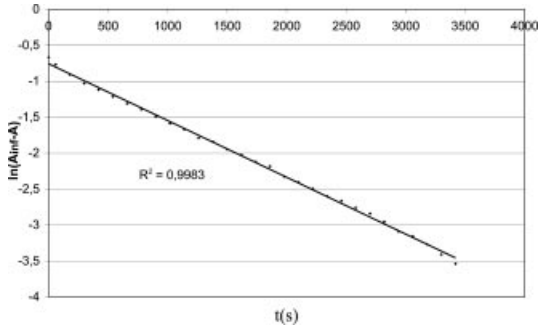


Figure 11. First-order plot based on the absorption change at 350 nm (P-core) for the reaction of **3** at –80 °C with $O_2$.

Table 3. Kinetic data for the formation of copper–dioxygen species (first-order kinetics).[28b]

| Compound | $k_1$ [$s^{-1}$] | $\Delta H^{\ddagger}$ [kJ $mol^{-1}$] | $\Delta S^{\ddagger}$ [J $mol^{-1}$ $K^{-1}$] |
|---|---|---|---|
| $[Cu_2(btmgp)_2][PF_6]_2$ (**1**) | $1.6(1)\times10^{-1}$ | 9(1) | –210(5) |
| $[Cu_2(DPipG_2p)_2][PF_6]_2$ (**2**) | $6.3(3)\times10^{-5}$ | 42(1) | –104(3) |
| $[Cu_2(DMPG_2p)_2][PF_6]_2$ (**3**) | $7.9(3)\times10^{-4}$ | 12(1) | –230(2) |

In comparison with **1** and **3**, complex **2** shows a higher activation enthalpy and a smaller negative activation entropy, which can be traced back to the steric demands of the piperidyl units.

## Electrochemistry

The copper(I) complexes **1**–**4** were also investigated cyclovoltammetrically to determine their redox activities. In the course of these measurements, irreversible oxidation waves at about –0.2 V attributable to the oxidation of $Cu^{I}$ to $Cu^{II}$ are observed for all the complexes (Table 4). This behaviour is not surprising as the initially linear coordination of $Cu^{I}$ requires subsequent rearrangement processes on changing the oxidation state of copper.

  

Table 4. Cyclovoltammetric data (MeCN/TBAP, 2 mm glassy carbon/NHE, $v$ = 100 mV s$^{-1}$, 25 °C).

| Copper complex (+1/+2) | $E_{ox}$ [V] |
|---|---|
| $[Cu_2(btmgp)_2][PF_6]_2$ (**1**) | –0.18 |
| $[Cu_2(DPipG_2p)_2][PF_6]_2$ (**2**) | –0.29 |
| $[Cu_2(DMPG_2p)_2][PF_6]_2$ (**3**) | –0.21 |
| $[Cu_2(DMEG_2p)_2][PF_6]_2$ (**4**) | –0.23 |

Interestingly, no correlation between the oxidation potentials of the copper(I) complexes **1**–**4** and their abilities to stabilise P- or O-core complexes could be found.

### Mechanism of the Reaction with Oxygen

The observed reaction with molecular oxygen has to be associated with a rearrangement of the bis(guanidine) ligands because the target area of this reaction is affected by significant H···H interactions between protons belonging to adjacent propylene spacers. This interaction is shown by the dashed line in Figure 4 (complex cation **2**). The corresponding ligand conformation represents the maximum stretch of the propylene spacer, which leads to a maximum intraligand N···N separation of 4.821 Å. On going to shorter N···N separations, as realised in the complex cations **1**, **3** and **4**, the propylene chain folds up and allows longer H···H contacts, as can be seen from Table 1 and Figures 3, 5 and 6, respectively. This would principally facilitate potential oxygen insertion, but is in contradiction with the requirements of the resulting $N_2Cu_2O_2N_2$ moiety, which demands intraligand N···N distances of at least 5.5 Å.[27c] Thus, the situation under discussion does not allow any insertion of oxygen into this region without rearrangement of the ligands.

Based on the kinetic data, we propose the following mechanism for the reaction with molecular oxygen (Scheme 4): the $Cu^I$ precursor (complex **a**) reacts in a sequence of first-order reactions with an excess of dioxygen to form the P-core complex. The oxygen uptake within step **A** is rate-determining. In the cases of **1** and **2**, the P-core complexes are less stable than their O-core counterparts, so that the reaction proceeds immediately via step **B**. In the case of **3**, the P-core complex is more stable, and its formation was investigated kinetically.

Reaction step **A** also includes the rearrangement of the bis(guanidine) moieties from nonchelating ligands into chelating ones. The corresponding reaction path is currently under investigation.

### σ-Donor and π-Acceptor Capabilities of the Ligands

In order to explain the reaction behaviour of the copper(I) complexes with molecular oxygen, we have to look at the special coordination properties of the guanidine ligands described above. The dihedral angles within the guanidine moieties are decisive for the discussion of these coordination properties (vide supra). Depending on the residues attached to the guanidine systems, the resulting $Cu_2O_2$ species

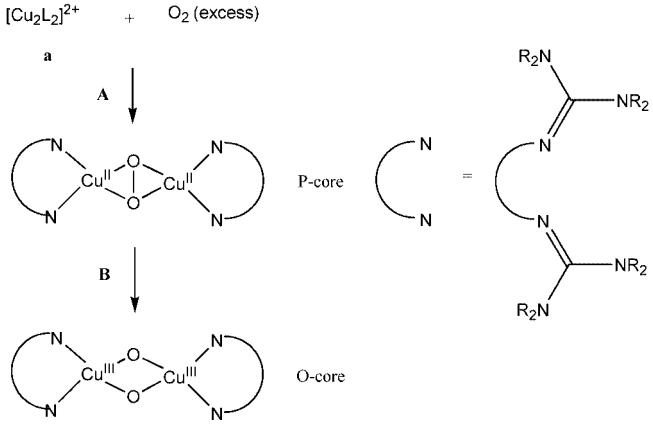


Scheme 4. Proposed mechanism of the reaction of **1**–**4** with dioxygen.

are either bis(μ-oxo)dicopper(III) or μ-η$^2$:η$^2$-peroxodicopper(II) complexes, or mixtures of both. The direction in which the equilibrium is driven depends on the degree of planarisation of the guanidine moieties. Within a guanidine residue, the observed structure is predominantly the result of an interplay of two major driving forces, one of them determined by electronic and the other by steric interactions.

Both types of interaction are competing against each other: as the p-orbitals of the peripheral $N^{amine}C_3$ portions search for reasonably good π-interactions with the central $CN_3$ unit, this prerequisite demands one common plane containing all the involved C and N atoms. On the other hand, the spatial demands of the substituents at the amine nitrogen atoms require propeller-like twists of the $NC_3$ portions around their N–$C^{imine}$ bonds, which thus prevents a coplanar arrangement with the central $CN_3$ group. Furthermore, we observed pyramidalisation tendencies of the peripheral $N^{amine}C_3$ portions, which are amplified if both N atoms are part of a heterocyclic ring, as in $DMPG_2p$ and $DMEG_2p$. The degree of pyramidalisation depends on the steric strain in the heterocycle but has no influence on the coordination properties.

It turned out that the result of the interplay between electronic (π-p conjugation) and steric forces (repulsion of the substituents, Figure 12) is decisive for the equilibrium between the bis(μ-oxo)- and the μ-η$^2$:η$^2$-peroxodicopper core. Small dihedral angles between adjacent $N^{amine}C_3$ and $CN_3$ units, indicative of a good conjugation of the π-orbitals in the guanidine moiety, favour the μ-η$^2$:η$^2$-peroxodicopper core, whereas moderately larger ones induce a shift of the equilibrium towards the formation of the bis(μ-oxo)dicopper state.

A bonding description of the P-core has been developed by a detailed correlation of spectral features, structural parameters and theoretical calculations by Solomon et al.[9] Furthermore, it is reported that strictly σ-donating ligands should be better suited to stabilise O-core complexes, whereas ligands with π-acceptor properties should favour the formation of their P-core counterparts.[2a,3a]

  

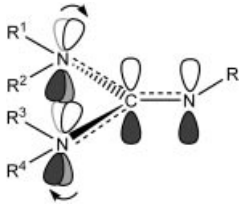

Figure 12. Competition of p-π conjugation and steric repulsion within the guanidine centre; arrows indicate twist from ideal conjugation (pale grey).

The bonding situation comprising a bis(guanidine) ligand attached to the $\{Cu_2O_2\}^{2+}$ core portion is illustrated in Scheme 5. In an attempt to elucidate the principal factors that control the P-core/O-core equilibrium, we correlated the degree of conjugation within the guanidine moiety with the reaction behaviour of the corresponding copper(I) complex towards oxygen. This correlation applies to bis(guanidine) ligands with propylene backbones. In the σ-plane (Scheme 5, left), the interaction of the σ-lobes of the coordinating imine nitrogen atoms with the $Cu^{II}$ $d_{x^2-y^2}$ orbital is denoted. Orthogonally to the σ-plane, the empty π*-orbitals (Scheme 5, right) of the guanidine moieties, representing the LUMO, possess the correct symmetry to accept electron density from the filled $d_{xz}$ and $d_{yz}$ orbitals of $Cu^{II}$. In the next step, electron density from the peroxide $\pi_v$*-orbital can now be transferred into the partially depleted $d_{xz}$ and $d_{yz}$ orbitals of $Cu^{II}$. At this stage, the degree of p-π conjugation within the guanidine system is of interest. Enhanced p-π overlap lowers the energy of the LUMO of the guanidine residue and makes it more accessible for π-back-donation. In consequence, small modifications of the ligand geometries that change the guanidine conjugation are suited to influence the equilibrium between P- and O-core complex states. In the ligands $DMPG_2p$ and $DMEG_2p$, the alkylene linkers tie the amine nitrogen atoms together and the average guanidine dihedral angles are therefore very small (vide supra). The guanidine conjugation is thus enhanced. However, in btmgp and $DPipG_2p$ the $NR_2$ moieties are twisted around their $N^{amine}$–$C^{imine}$ bonds, and the guanidine conjugation is hindered. For that reason, the LUMO is raised in energy, and back-donation is diminished. Now, the σ-donating effect of the imine nitrogen atoms dominates the coordination and the O-core is stabilised.

## Conclusions

The novel dipod ligand bis(dimethylethyleneguanidino)-propane ($DMEG_2p$) has been synthesised for use in biomimetic coordination chemistry. $DMEG_2p$ belongs to a new class of bis(guanidine) ligands whose $Cu^I$ complexes are well suited to activate molecular oxygen. Due to their ability to delocalise the positive charge over the guanidine moiety, these ligands are able to stabilise high metal oxidation states, which are established in a variety of copper complexes containing the $\{Cu_2O_2\}^{2+}$ core portion. The analysis of the bonding situation comprising this site attached to a bis(guanidine) residue reveals that the coordination properties of the imine N-donor atoms depend on the substitution pattern within the guanidine moieties. Thus, it is possible to influence the reactivity of the bis(guanidine)copper(I) complexes towards molecular oxygen directly by introducing appropriately designed substituents. Sterically demanding alkyl groups raise the energy of the LUMO, which has the appropriate symmetry to accept electrons from the $\{Cu_2O_2\}^{2+}$ core portion and thus destabilise the P-core state within these complexes. On the other hand, integrating both amine groups of a guanidine residue into a five- or six-membered ring favours the P-core over the O-core state by strengthening the π-conjugation within the ligand and thus lowering the energy of the LUMO. Based on these interrelations between steric features of the ligands and the electron distribution within the $\{Cu_2O_2\}^{2+}$ core portions of dinuclear $Cu_2O_2$ complexes, new insights into the mechanism of dioxygen activation are provided and strategies towards ligand modification can be developed which are directed towards tailored reaction systems capable of hydroxylating substrates in pre-defined positions.

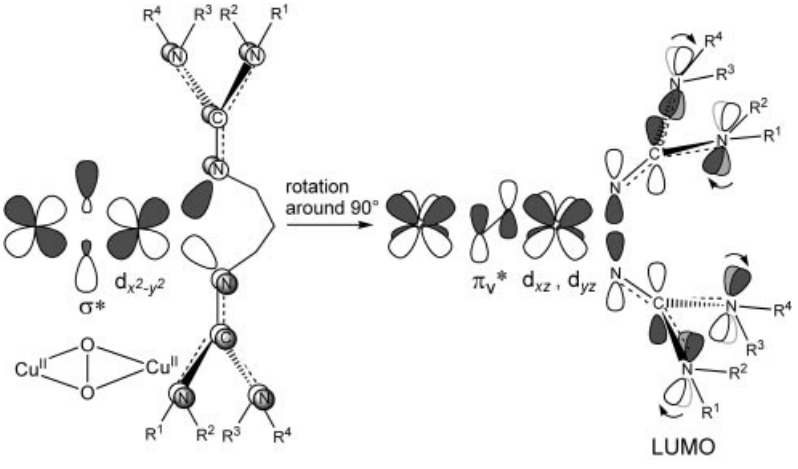


Scheme 5. Bonding situation comprising a bis(guanidine) ligand attached to the $\{Cu_2O_2\}^{2+}$ core portion.

  

## Experimental Section

**General Remarks:** All manipulations were performed under pure dinitrogen (99.996%) dried with $P_4O_{10}$ using Schlenk techniques or a glovebox and with absolute solvents. Solvents were purified according to literature procedures and also kept under nitrogen. Triethylamine and 1,3-diaminopropane were used as purchased from Fluka. $[Cu(MeCN)_4][PF_6]$, the Vilsmeier salts and the ligands btmgp, $DMPG_2p$ and $DPipG_2p$ were prepared according to literature procedures.[24,27]

**Physical Measurements:** Spectra were recorded with the following spectrometers: NMR: Bruker AMX 300 and Avance 500, respectively. IR: Nicolet P510. UV: Perkin–Elmer Lambda 45 in combination with the Hellma UV/Vis low-temperature fibre optic interface (1-cm path length cell), excess $O_2$, Lauda RL 6 CP cryostat. Copper(I) solutions were transferred into the UV low-temperature cell with a steel capillary under argon pressure. MS (EI, 70 eV): Saturn 2. The elemental analysis for $DMEG_2p$ was performed with a Perkin–Elmer 2400 analysator. Microanalyses for **1**–**4** were performed at the Mikroanalytisches Labor, Ilse Beetz, Kronach, Germany. Cyclic voltammetry (CV) was performed with the electrochemical device Metrohm E 505 equipped with a potentiostat Model VersaStat by EG&G in combination with the PC program Electrochemical Analysis Software 3.0 Model 250 by EG&G. The electrochemical cell was operated under argon, with glassy carbon, glassy carbon and saturated Ag/AgCl serving as working, counter and reference electrodes, respectively. CV curves were obtained at scan rates of 100 mV s$^{-1}$ at 25 °C in MeCN/0.1 M $n$Bu$_4$NPF$_6$. As the complexes are extremely air-sensitive, the copper(I) solutions were transferred into the CV cell with a steel capillary under argon pressure.

***Caution!*** Phosgene is a severe toxic agent that can cause pulmonary embolism and, in the case of prolonged exposure, may be lethal. Use only in a well-ventilated fume hood.

**Chloro-*N*,*N*′-bis(1-piperidyl)formamidinium Chloride:** According to a literature procedure,[27b] phosgene was passed at 0 °C through a solution of Bis(1-piperidyl) ketone (Aldrich, 12.5 g, 63.8 mmol) in dry MeCN (200 mL) for 30 min. The reaction mixture was stirred at room temperature for 6 h and at 40 °C for another 36 h. After the mixture had cooled down to room temperature, the solvent was evaporated under reduced pressure in order to obtain the product as colourless, slowly crystallising oil. Yield: ca.70% (112 g, 44.7 mmol).

**Chloro-*N*,*N*′-ethylene-*N*,*N*′-dimethylformamidinium Chloride:** Phosgene was passed at 0 °C through a solution of 1,3-dimethyl-2-imidazolidinone (Fluka, 68.5 g, 600 mmol) in dry toluene (300 mL) for 50 min. The reaction mixture was stirred at room temperature for 2 h and at 40 °C for another 12 h. After the mixture had cooled down to room temperature, the white precipitate formed was collected by filtration, washed three times with dry diethyl ether, and dried in vacuo. Yield: 95% (96 g, 570 mmol).

***N*,*N*′-Bis(1,3-dimethylimidazolidin-2-ylidene)propane-1,3-diamine [Bis(dimethylethyleneguanidino)propane, $DMEG_2p$]:** A solution of chloro-*N*,*N*′-ethylene-*N*,*N*′-dimethylformamidinium chloride (6.76 g, 40 mmol) in dry MeCN (80 mL) was added dropwise, with vigorous stirring, to an ice-cooled solution of 1,3-diaminopropane (1.48 g, 20 mmol) and triethylamine (5.57 mL, 4.04 g, 40 mmol) in dry MeCN (40 mL). After 3 h at reflux, a solution of NaOH (1.6 g, 40 mmol) in water (10 mL) was added. Solvents and $Et_3N$ were then evaporated under vacuum. In order to deprotonate the bis(hydrochloride), 50 wt% KOH (aq., 25 mL) was added and the free base was extracted into the MeCN phase (3 × 25 mL). The organic phase was dried with $Na_2SO_4$ on charcoal. After filtration through Celite, the solvent was evaporated under reduced pressure. The pure product was obtained as a colourless oil which crystallised after 2 months as needles suitable for X-ray diffraction; yield: 95% (5.05 g, 19 mmol). $^1$H NMR (500 MHz, $CDCl_3$, 25 °C): $\delta$ = 1.57 (m, 2 H, $CH_2$), 2.60 (s, 12 H, $CH_3$), 2.95 (br., 8 H, $CH_2$), 3.26 (t, $^3J$ = 6.7 Hz, 4 H, $CH_2$) ppm. $^{13}$C NMR (125 MHz, $CDCl_3$, 25 °C): $\delta$ = 32.1 ($C_a$), 36.3 ($CH_3$), 45.0 ($C_b$), 49.3 ($CH_2$), 157.3 ($C_{gua}$) ppm. IR (film NaCl): $\tilde{\nu}$ = 2931 s, 2831 s, 1660 vs. [ν(C=N)], 1651 vs. [ν(C=N)], 1485 s, 1435 m, 1422 m, 1384 m, 1336 w, 1263 m, 1241 w, 1113 w cm$^{-1}$. EI-MS: *m*/*z* (%) = 266.2 (39) [M$^+$], 249 (4) [M$^+$ – $CH_3$], 205 (5), 152 (10), 140 (60) [$CH_2CH_2N{=}CN_2C_4H_{10}^+$], 126 (80) [$CH_2N{=}CN_2C_4H_{10}^+$], 114 (100) [$H_2N{=}CN_2C_4H_{10}^+$], 98 (32), 84 (25), 70 (24). $C_{13}H_{26}N_6$ (266.4): calcd. C 58.61, H 9.84, N 31.55; found C 58.93, H 9.58, N 31.49.

**$[Cu_2(btmgp)_2][PF_6]_2$ (1):** $[Cu(MeCN)_4][PF_6]$ (372 mg, 1 mmol) was added to a stirred solution of btmgp (284 mg, 1.05 mmol) in MeCN (15 mL). After 30 min of stirring, diethyl ether (20 mL) was added to obtain the colourless product, yield: 90% (430 mg). Crystals suitable for X-ray diffraction were grown by slow diffusion of diethyl ether into an MeCN solution of **1**. $^1$H NMR (300 MHz, $CDCl_3$, 25 °C): $\delta$ = 2.01 (s, MeCN), 2.28 (m, 2 H, $H_b$), 2.89 (s, 12 H, $CH_3$), 2.91 (s, 12 H, $CH_3$), 3.32 (m, 4 H, $H_a$) ppm. IR (KBr): $\tilde{\nu}$ = 3435 w, 2953 m [ν(CH)], 2931 m [ν(CH)], 2881 m [ν(CH)], 2853 w [ν(CH)], 1564 s [ν(C=N)], 1558 s [ν(C=N)], 1539 s [ν(C=N)], 1477 m [δ(CH)], 1464 m [δ(CH)], 1456 m, 1427 m, 1416 m, 1408 m, 1398 s [ν(C=N)], 1362 m [ν(C=N)], 1337 vw, 1240 w, 1169 m [ν(C=N)], 1161 w, 1123 w, 1070 m [ν(C=N)], 1024 w, 1011 w, 899 w, 876 m, 839 vs, 779 w, 557 m cm$^{-1}$. UV/Vis ($CH_2Cl_2$): $\lambda_{max}$ (ε) = no bands; shoulder at 360 nm (233 M$^{-1}$ cm$^{-1}$). $C_{26}H_{60}Cu_2F_{12}N_{12}P_2$ (957.9): calcd. C 32.60, H 6.31, N 17.55; found C 32.66, H 6.39, N 17.52.

**$[Cu_2(DPipG_2p)_2][PF_6]_2$ (2):** $[Cu(MeCN)_4][PF_6]$ (372 mg, 1 mmol) was added to a stirred solution of $DPipG_2p$ (452 mg, 1.05 mmol) in MeCN (15 mL). After 30 min of stirring, diethyl ether (20 mL) was added to obtain the colourless product, yield: 82% (524 mg). Crystals suitable for X-ray diffraction were grown by slow diffusion of diisopropyl ether into an MeCN solution of **2**. $^1$H NMR (500 MHz, $CD_3CN$, 25 °C): $\delta$ = 1.48–1.58 (m, 24 H, Pip-$CH_2$), 1.71 (q, $^3J$ = 7.0 Hz, 2 H, $CH_2$), 3.05 (t, $^3J$ = 7.0 Hz, 16 H, Pip-$CH_2$), 3.55 (t, 4 H, $CH_2$) ppm. $^{13}$C NMR (125 MHz, $CD_3CN$, 25 °C): $\delta$ = 24.0 (Pip), 25.2 (Pip), 25.6 (Pip) 33.8 ($C_a$), 47.6 ($C_b$), 49.3 (Pip), 160.2 ($C_{quat.}$) ppm. IR (KBr): $\tilde{\nu}$ = 2934 m, 2852 m, 1626 s [ν(C=N)], 1554 s [ν(C=N)], 1548 s [ν(C=N)], 1491 m [ν(C=N)], 1440 m, 1372 m, 1341 w, 1261 w, 1253 m 1236 w, 1211 w, 1203 w, 1163 m, 1114 w, 1078 m, 1023 m, 1016 w, 985 w, 907 w, 839 vs. [ν(P–F)], 787 m, 705 w, 581 w, 555 m cm$^{-1}$. $C_{50}H_{92}Cu_2F_{12}N_{12}P_2$ (1278.4): calcd. C 46.98, H 7.25, N 13.15; found C 46.99, H 7.22, N 13.19.

**$[Cu_2(DMPG_2p)_2][PF_6]_2$ (3):** $[Cu(MeCN)_4][PF_6]$ (372 mg, 1 mmol) was added to a stirred solution of $DMPG_2p$ (308.7 mg, 1.05 mmol) in MeCN (15 mL). After 30 min of stirring, diethyl ether (20 mL) was added to obtain the colourless product, yield: 86% (433 mg). Crystals suitable for X-ray diffraction were grown by slow diffusion of diisopropyl ether into an MeCN solution of **3**. $^1$H NMR (500 MHz, $CD_3CN$, 25 °C): $\delta$ = 1.62 (m, 2 H, $CH_2$), 1.71 (m, 4 H, $CH_2$), 2.95 (s, 12 H, $CH_3$), 3.15 (m, 8 H, $CH_2$) ppm. $^{13}$C NMR (125 MHz, $CD_3CN$, 25 °C): $\delta$ = 22.3 ($CH_2$), 34.8 ($C_a$), 40.1 ($CH_3$), 46.3 ($C_b$), 49.7 ($CH_2$), 160.6 ($C_{quat.}$) ppm. IR (KBr): $\tilde{\nu}$ = 2953 s, 2919 s, 2864 s, 2831 m, 1564 vs. [ν(C=N)], 1552 vs. [ν(C=N)], 1537 vs. [ν(C=N)], 1473 s, 1453 s, 1419 s, 1403 vs. [ν(C=N)], 1376 s, 1354 s, 1325 s, 1313 s, 1272 w, 1236 s, 1206 w, 1162 w, 1113 w, 1084 m, 1050 m, 1014 m, 837 vs. [ν(P–F)], 769 s, 557 s, 511 m cm$^{-1}$.

  

Table 5. Crystal data for compounds **1**–**4**.

| | **1** | **2** | **3** | **4** |
|---|---|---|---|---|
| Empirical formula | $C_{26}H_{60}Cu_2F_{12}N_{12}P_2$ | $C_{50}H_{92}Cu_2F_{12}N_{12}P_2$ | $C_{30}H_{60}Cu_2F_{12}N_{12}P_2$ | $C_{30}H_{58}Cu_2F_{12}N_{14}P_2$ |
| Formula mass | 957.88 | 1278.38 | 1005.92 | 1031.92 |
| Crystal size [mm] | 0.25×0.20×0.18 | 0.22×0.15×0.10 | 0.40×0.40×0.18 | 0.20×0.12×0.10 |
| Crystal system | monoclinic | monoclinic | triclinic | triclinic |
| Space group | $P2_1/n$ | $C2/c$ | $P\bar{1}$ | $P\bar{1}$ |
| $a$ [Å] | 8.177(1) | 30.457(6) | 9.577(1) | 7.831(1) |
| $b$ [Å] | 15.574(3) | 9.139(2) | 10.420(1) | 11.650(1) |
| $c$ [Å] | 16.218(3) | 21.278(4) | 10.703(1) | 12.474(1) |
| $\alpha$ [°] | 90 | 90 | 103.29(1) | 78.02(1) |
| $\beta$ [°] | 96.47(1) | 95.38(1) | 96.94(1) | 81.70(1) |
| $\gamma$ [°] | 90 | 90 | 90.61(1) | 81.18(1) |
| $V$ [Å$^3$] | 2052.3(6) | 5896.6(7) | 1031.1(6) | 1092.5(6) |
| $Z$ | 2 | 4 | 1 | 1 |
| $D_{calcd.}$ [g cm$^{-3}$] | 1.550 | 1.440 | 1.620 | 1.568 |
| $\mu$(Mo-$K_\alpha$) [mm$^{-1}$] | 1.205 | 0.859 | 1.204 | 1.140 |
| Temperature [K] | 150(2) | 120(2) | 150(2) | 120(2) |
| Data collection range $\Theta$ [°] | 1.82 to 28.28 | 1.34 to 28.52 | 1.97 to 26.37 | 1.68 to 28.24 |
| $h,k,l$ | –10/9, –19/20, –21/20 | ± 40, –11/12, –28/22 | ±11, ±13, ±13 | ±10, –14/15, ±16 |
| No. of reflections measured | 12491 | 26613 | 11105 | 14028 |
| No. of unique data | 4731 | 7392 | 4181 | 5385 |
| Parameters | 252 | 354 | 266 | 276 |
| $R_1$ [$I \geq 2\sigma(I)$] | 0.046 | 0.046 | 0.026 | 0.044 |
| $wR_2$ (all data) | 0.115 | 0.079 | 0.069 | 0.095 |
| Min/max $\Delta F$ [e Å$^{-3}$] | –0.42/0.91 | –0.45/0.40 | –0.18/0.34 | –0.57/0.74 |

$C_{30}H_{60}Cu_2F_{12}N_{12}P_2$ (1005.9): calcd. C 35.82, H 6.01, N 16.71; found C 35.64, H 6.07, N 16.58.

**$[Cu_2(DMEG_2p)_2][PF_6]_2$·2MeCN (4):** $[Cu(MeCN)_4][PF_6]$ (372 mg, 1 mmol) was added to a stirred solution of $DMEG_2p$ (279 mg, 1.05 mmol) in MeCN (15 mL). After 30 min of stirring, diethyl ether (20 mL) was added to obtain the colourless product, yield: 82% (389 mg). Crystals suitable for X-ray diffraction were grown by slow diffusion of diisopropyl ether into an MeCN solution of **4**. $^1$H NMR (500 MHz, $CD_3CN$, 25 °C): $\delta$ = 1.82 (m, 2 H, $CH_2$), 3.00 (s, 12 H, $CH_3$), 3.46 (br., 8 H, $CH_2$), 3.65 (t, $^3J$ = 7.1 Hz, 4 H, $CH_2$) ppm. $^{13}$C NMR (125 MHz, $CD_3CN$, 25 °C): $\delta$ = 35.0 ($C_a$), 35.6 ($CH_3$), 45.2 ($C_b$), 49.2 ($CH_2$), 162.4 ($C_{gua}$) ppm. IR (KBr): $\tilde{\nu}$ = 2929 s, 2894 s, 1631 s [$\nu$(C=N)], 1601 vs. [$\nu$(C=N)], 1512 m [$\nu$(C=N)], 1490 m, 1459 m, 1419 m, 1400 m, 1345 w, 1300 s, 1232 w, 1208 w, 1121 w, 1076 w, 1034 w, 970 vw, 839 vs. [$\nu$(P–F)], 723 w, 646 w, 557 vs, 484 w cm$^{-1}$. $C_{26}H_{52}Cu_2F_{12}N_{12}P_2$ (949.8, after removing the solvent in vacuo): calcd. C 32.88, H 5.52, N 17.70; found C 33.19, H 5.28, N 17.93.

**Crystal Structure Analyses:** Crystal data for compounds **1**–**4** are presented in Table 5. X-ray diffraction data were collected with a Bruker-AXS SMART APEX CCD diffractometer using Mo-$K_\alpha$ radiation ($\lambda$ = 0.71073 Å). Data reduction and absorption correction were performed with SAINT and SADABS.[29] The structures were solved by direct and conventional Fourier methods and all non-hydrogen atoms refined anisotropically with full-matrix least-squares procedures based on $F^2$ (SHELXTL[29]). Hydrogen atoms were derived from difference Fourier maps and placed at idealised positions, riding on their parent C atoms, with isotropic displacement parameters $U_{iso}$(H) = 1.2$U_{eq}$(C) and 1.5$U_{eq}$(C methyl). All methyl groups were allowed to rotate but not to tip. Compound **4** contains two MeCN solvent molecules per unit cell. CCDC-273408 (**1**), -273409 (**2**), -273410 (**3**), and -273411 (**4**) contain the supplementary crystallographic data for this paper. These data can be obtained free of charge from The Cambridge Crystallographic Data Centre via www.ccdc.cam.ac.uk/data_request/cif.

**Supporting Information Available** (see footnote on the first page of this article): Figures S1, S2 and S3 showing Eyring plots for **1**, **2** and **3**, respectively.

## Acknowledgments

We gratefully acknowledge the financial support of the Fonds der Chemischen Industrie (FCI), the Deutsche Forschungsgemeinschaft and the Bundesministerium für Bildung und Forschung. S. H.-P. thanks the FCI for a fellowship.

[1] a) E. A. Lewis, W. B. Tolman, *Chem. Rev.* **2004**, *104*, 1047; b) S. T. Prigge, B. A. Eipper, R. E. Mains, L. M. Amzel, *Science* **2004**, *304*, 864; c) E. I. Tocheva, F. I. Rosell, A. G. Mauk, M. E. P. Murphy, *Science* **2004**, *304*, 867.
[2] a) L. M. Mirica, X. Ottenwaelder, T. D. P. Stack, *Chem. Rev.* **2004**, *104*, 1013; b) H.-C. Liang, M. J. Henson, L. Q. Hatcher, M. A. Vance, C. X. Zhang, D. Lahti, S. Kaderli, R. D. Sommer, A. L. Rheingold, A. D. Zuberbühler, E. I. Solomon, K. D. Karlin, *Inorg. Chem.* **2004**, *43*, 4115.
[3] a) L. Que, Jr., W. B. Tolman, *Angew. Chem.* **2002**, *114*, 1160; *Angew. Chem. Int. Ed.* **2002**, *41*, 1114; b) P. L. Holland, W. B. Tolman, *Coord. Chem. Rev.* **1999**, *190–192*, 855.
[4] T. D. P. Stack, *Dalton Trans.* **2003**, 1881.
[5] a) E. I. Solomon, P. Chen, M. Metz, S.-K. Lee, A. E. Palmer, *Angew. Chem.* **2001**, *113*, 4702; *Angew. Chem. Int. Ed.* **2001**, *40*, 4570; b) R. H. Holm, P. Kennepohl, E. I. Solomon, *Chem. Rev.* **1996**, *96*, 2239; c) J. A. Guckert, M. D. Lowery, E. I. Solomon, *J. Am. Chem. Soc.* **1995**, *117*, 2817.
[6] A. G. Blackman, W. B. Tolman, *Struct. Bonding (Berlin)* **2000**, *97*, 179.
[7] a) K. A. Magnus, H. Ton-That, J. E. Carpenter, *Chem. Rev.* **1994**, *94*, 727; b) K. A. Magnus, B. Hazes, H. Ton-That, C. Bonaventura, J. Bonaventura, W. G. L. Hol, *Proteins: Struct. Funct. Genet.* **1994**, *19*, 302.
[8] M. E. Cuff, K. I. Miller, K. E. Vanholde, W. A. Hendrickson, *J. Mol. Biol.* **1998**, *278*, 855.

  

[9] a) E. I. Solomon, U. M. Sundaram, T. E. Machonkin, *Chem. Rev.* **1996**, *96*, 2563; b) M. J. Baldwin, D. E. Root, J. E. Pate, K. Fujisawa, N. Kitajima, E. I. Solomon, *J. Am. Chem. Soc.* **1992**, *114*, 10421.
[10] A. Rompel, H. Fischer, D. Meiwes, K. Buldt-Karentzopoulos, R. Dillinger, F. Tuczek, H. Witzel, B. Krebs, *J. Biol. Inorg. Chem.* **1999**, *4*, 56.
[11] a) C. Gerdemann, C. Eicken, B. Krebs, *Acc. Chem. Res.* **2002**, *35*, 183; b) T. Klabunde, C. Eicken, J. C. Sacchettini, B. Krebs, *Nat. Struct. Biol.* **1998**, *5*, 1084.
[12] J. P. Klinman, *Chem. Rev.* **1996**, *96*, 2541.
[13] C. M. Wilmot, J. Hajdu, M. J. McPherson, P. F. Knowles, S. E. V. Phillips, *Science* **1999**, *286*, 1724.
[14] a) N. Kitajima, Y. Moro-oka, *Chem. Rev.* **1994**, *94*, 737; b) N. Kitajima, K. Fujisawa, C. Fujimoto, Y. Moro-oka, S. Hashimoto, T. Kitagawa, K. Toriumi, K. Tatsumi, A. Nakamura, *J. Am. Chem. Soc.* **1992**, *114*, 1277.
[15] K. Fujisawa, M. Tanaka, Y. Moro-oka, N. Kitajima, *J. Am. Chem. Soc.* **1994**, *116*, 12079.
[16] V. Mahadevan, Z. Hou, A. P. Cole, D. E. Root, T. P. Lal, E. I. Solomon, T. D. P. Stack, *J. Am. Chem. Soc.* **1997**, *119*, 11996.
[17] L. M. Mirica, M. Vance, D. Jackson-Rudd, B. Hedman, K. O. Hodgson, E. I. Solomon, T. D. P. Stack, *J. Am. Chem. Soc.* **2002**, *124*, 9332.
[18] a) A. P. Cole, D. E. Root, P. Mukherjee, E. I. Solomon, T. D. P. Stack, *Science* **1996**, *273*, 1848; b) M. Taki, S. Teramae, S. Nagatomo, Y. Tachi, T. Kitagawa, S. Itoh, S. Fukuzumi, *J. Am. Chem. Soc.* **2002**, *124*, 6367.
[19] P. L. Holland, K. R. Rodgers, W. B. Tolman, *Angew. Chem.* **1999**, *111*, 1210; *Angew. Chem. Int. Ed.* **1999**, *38*, 1139.
[20] V. Mahadevan, J. L. DuBois, B. Hedman, K. O. Hodgson, T. D. P. Stack, *J. Am. Chem. Soc.* **1999**, *121*, 5583.
[21] S. Mahapatra, V. G. Young, Jr., S. Kaderli, A. D. Zuberbühler, W. B. Tolman, *Angew. Chem.* **1997**, *109*, 125–127; *Angew. Chem. Int. Ed. Engl.* **1997**, *36*, 130.
[22] S. Itoh, T. Kondo, M. Komatsu, Y. Oshiro, C. Li, N. Kanehisa, Y. Kai, S. Fukuzumi, *J. Am. Chem. Soc.* **1995**, *117*, 4714.
[23] S. Itoh, H. Nakao, L. M. Berreau, T. Kondo, M. Komatsu, S. Fukuzumi, *J. Am. Chem. Soc.* **1998**, *120*, 2890.
[24] a) S. Pohl, M. Harmjanz, J. Schneider, W. Saak, G. Henkel, *J. Chem. Soc., Dalton Trans.* **2000**, 3473; b) S. Pohl, M. Harmjanz, J. Schneider, W. Saak, G. Henkel, *Inorg. Chim. Acta* **2000**, *311*, 106.
[25] S. Herres, A. J. Heuwing, U. Flörke, J. Schneider, G. Henkel, *Inorg. Chim. Acta* **2005**, *358*, 1089.
[26] a) H. Wittmann, A. Schorm, J. Sundermeyer, *Z. Anorg. Allg. Chem.* **2000**, *626*, 1583; b) V. Raab, J. Kipke, O. Burghaus, J. Sundermeyer, *Inorg. Chem.* **2001**, *40*, 6964; c) H. Wittmann, V. Raab, A. Schorm, J. Plackmeyer, J. Sundermeyer, *Eur. J. Inorg. Chem.* **2001**, 1937.
[27] a) S. Herres, U. Flörke, G. Henkel, *Acta Crystallogr., Sect. C* **2004**, *60*, o358; b) W. Kantlehner, E. Haug, W. W. Mergen, P. Speh, T. Maier, J. J. Kapassakalidis, H.-J. Bräuner, H. Hagen, *Liebigs Ann. Chem.* **1984**, *1*, 108; c) S. Herres, U. Flörke, G. Henkel, *Acta Crystallogr., Sect. C* **2004**, *60*, m659.
[28] a) Resonance-Raman spectra are severely affected by fluorescence emission and thus not suited to contribute to the P-core/O-core question. b) The *k* values for **1**–**3** were determined five times for each temperature step of 5 K between 193 K and 233 K. The average *k* values were calculated and plotted in an Eyring plot (see Supporting Information). The temperature deviation was estimated to be 0.2 K.
[29] SAINT (version 6.02), SHELXTL (version 6.10), SADABS (version 2.03), Bruker AXS, Inc., Madison, Wisconsin, USA, **2002**..

Received: September 30, 2004
Published Online: August 31, 2005

  